Article

Not peer-reviewed version

Polysulfone/MMT Clay Mixed Matrix Membranes for Efficient Diclofenac Removal and Improved Antifouling Performance in Wastewater Treatment

Zouhair Salah , Hajer Aloulou , Catia Algieri , Lasaad Dammak * , Raja Ben Amar *

Posted Date: 14 October 2025

doi: 10.20944/preprints202510.1117.v1

Keywords: montmorillonite; Polysulfone; mixed-matrix membrane; diclofenac removal; antifouling

 doi:10.20944/preprints202510.1117.v1

Article

Polysulfone/MMT Clay Mixed Matrix Membranes for Efficient Diclofenac Removal and Improved Antifouling Performance in Wastewater Treatment

Zouhair Salah [1], Hajer Aloulou [1,2], Catia Algieri [3], Lasaad Dammak [4,*] and Raja Ben Amar [1,*]

[1] Research Unit 'Advanced Technologies for Environment and Smart Cities', Faculty of Sciences of Sfax, University of Sfax, Tunisia
[2] Department of Chemical, Preparatory Institute for Engineering Studies of Gabes, University of Gabes, Gabes 6029, Tunisia
[3] Institute on Membrane Technology, National Research Council of Italy (ITM–CNR), Cubo 17C, Via Pietro Bucci, Rende 87036, Italy
[4] Université Paris-Est Créteil, CNRS, ICMPE, UMR 7182, 2 rue Henri Dunant, 94320 Thiais, France
* Correspondence: benamar.raja@yahoo.com (R. Ben Amar); dammak@u-pec.fr (L. Dammak)

Abstract

Due to industrialization and globalization, water sources are increasingly contaminated with drugs. Among the various methods available, adsorption remains one of the most widely used techniques for drug removal. This work was to develop polysulfone (PSF) membranes integrated with montmorillonite (MMT) clay. The fabricated membranes were subsequently evaluated for their performance in removing diclofenac (DCF) from aqueous solutions. The membranes were characterized using scanning electron microscopy (SEM), energy-dispersive X-ray spectroscopy (EDX), Fourier transform infrared spectroscopy (FTIR), contact angle measurements, as well as chemical and mechanical tests. Adding MMT at 1.5 and 2 wt% improved both hydrophilicity and mechanical strength. The natural hydrophilicity of MMT also accelerates the non-solvent/solvent exchange during phase inversion, resulting in higher porosity. These structural and surface modifications increased water permeability (7.5 $L.m^{-2}.h^{-1}.bar^{-1}$), achieved 79% DCF removal, and enhanced antifouling properties. However, increasing the MMT clay content to 2.5 wt% caused particle aggregation, which reduced membrane performance. Fouling resistance tests with bovine serum albumin (BSA) as a model foulant showed a rejection rate of 89% and a flux recovery ratio (FRR) above 82% using an optimized membrane. These findings demonstrate that PSF/MMT membranes can serve as promising candidates for sustainable pharmaceutical wastewater treatment.

Keywords: montmorillonite; Polysulfone; mixed-matrix membrane; diclofenac removal; antifouling

1. Introduction

Today, access to fresh and clean water remains one of the most pressing global challenges, drawing considerable attention from the scientific community [1]. Numerous pollutants found in aquatic environments exert harmful effects on ecosystems and human health, posing serious threats to the survival of marine organisms and other life forms [2]. Among these, pharmaceutical residues are particularly concerning, as they represent a major class of emerging contaminants discharged into water bodies, primarily from pharmaceutical industries [3,4]. Additional sources include biomedical waste from hospitals, human excreta, livestock treatments, and veterinary medicines [5,6]. Diclofenac (DCF), one of the most widely used non-steroidal anti-inflammatory drugs, is frequently detected in aqueous effluents [7]. Concentrations of DCF have been reported in municipal wastewater at levels reaching up to 57.16 $\mu g.L^{-1}$ [8,9]. This compound is associated with several adverse effects, including chronic headaches, gastric pain, chest discomfort, respiratory difficulties, fever, and allergic reactions

 doi:10.20944/preprints202510.1117.v1

[9]. Consequently, its removal from water has become a priority for researchers. Several treatment methods have been investigated for the elimination or degradation of pharmaceutical pollutants, including adsorption [10], ozonation [11], bio-sorption, advanced oxidation processes [12,13], coagulation and flocculation [14], and membrane processes [15,16].

Among various treatment techniques, the use of adsorbents for removing low concentrations of hazardous contaminants has shown superior performance compared to alternative methods [17]. Activated carbon is the most commonly employed commercial adsorbent; however, its high cost restricts large-scale applications [18]. To overcome these limitations, organic–inorganic hybrid materials have recently been developed to fabricate membranes with enhanced properties and broader application potential [13,14]. For instance, Salah et al. incorporated graphene oxide (GO) into a polysulfone (PSf) matrix to improve both water permeability and diclofenac (DCF) removal [19], while Chai et al. embedded Fe_3O_4/GO into PSf to enhance permeability and humic acid rejection [20]. A wide range of inorganic particles, including metal oxides, zeolites, and clays, has been introduced into membrane fabrication [21,22]. Among these, clay has attracted growing interest as a filler due to its low cost, abundance, environmental friendliness, and ability to significantly improve polymer properties even at low loading levels. Polymer–clay composites have been applied in numerous industrial, technological, and environmental fields [23], particularly in water treatment, where clay improves hydrophilicity and enhances pollutant removal efficiency [23].

Clay is considered one of the most promising fillers for membrane modification, owing to its high specific surface area and intrinsic hydrophilicity, and is the principal factor in improving membrane performance [24]. Montmorillonite (MMT), a layered aluminosilicate clay with a basal spacing of approximately 1 nm, is of particular interest [25]. Structurally, MMT consists of alternating layers of silica in tetrahedral coordination and alumina in octahedral coordination [26].

Despite its potential, relatively few studies have reported on PSF-Clay nanocomposites. Notably, two works employed the solution dispersion method with organophilic MMT as a filler [27,28], while another study investigated a PSF/cyanate ester/organophilic MMT blend [29]. Beyond PSf, polymer–clay nanocomposite (PCN) membranes have been widely explored in the context of fuel cells, particularly using Nafion combined with either protonated MMT [30] or sulfonated MMT [31]. Other combinations include sulfonated poly(ether ketone) with both organophilic and sulfonated MMT [32] as well as organophilic MMT blended into polyamide, poly(vinylidene fluoride), and poly-lactic acid, yielding membranes with improved physicochemical properties [33].

In this study, polysulfone–montmorillonite (PSF–MMT) mixed matrix membranes (MMMs) were prepared using the non-solvent induced phase separation (NIPS) method. The effect of MMT clay incorporation on the membranes' hydrophilicity, mechanical strength, water permeability, and morphology was systematically evaluated. Membrane performance was tested through the removal of diclofenac from water solution, while bovine serum albumin (BSA) served as a model foulant to assess the antifouling properties and flux recovery of the fabricated nanocomposite membranes.

Scheme 1 presents the conceptual framework of this work. It highlights the sequential approach adopted in this study: (i) fabrication of the PSF/MMT composite membranes through the phase inversion method, (ii) characterization of their physicochemical and morphological properties, and (iii) evaluation of their separation and antifouling performance. This workflow provides a clear overview of the experimental logic linking membrane structure to performance.

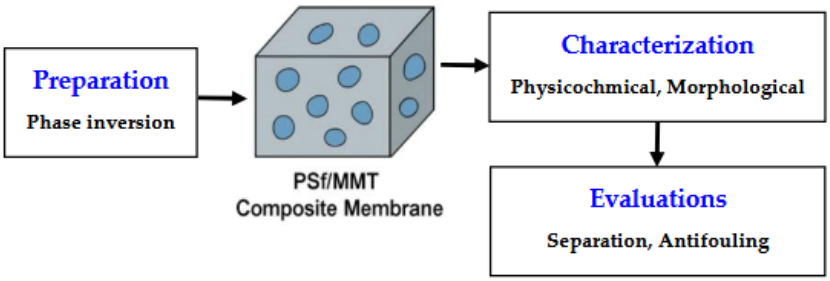

 doi:10.20944/preprints202510.1117.v1

Scheme 1. Conceptual representation of the PSF/MMT membrane development process, from fabrication to performance assessment for diclofenac removal.

2. Methodology

2.1. Chemicals and Reagents

Polysulfone (PSF, average molecular weight Mw = 22,000 g.mol^{-1}) and N-methyl-2-pyrrolidone (NMP, 99.7%) were purchased from Merck (Germany). NMP was used directly as a solvent for preparing the polymer solution. Montmorillonite clay (MMT) was purchased from Sigma-Aldrich (St Louis, MO, USA). Distilled water was used both as a non-solvent during membrane fabrication and for water flux measurements. Sodium hydroxide (NaOH), ethanol (C_2H_5OH), and diclofenac sodium (DCF, $C_{14}H_{10}Cl_2NNaO_2$) were also purchased from Sigma-Aldrich.

2.2. Membrane Preparation

Two types of membranes were fabricated: one based on pure polysulfone (PSF) and the other on polysulfone incorporated with montmorillonite (PSF/MMT) clay. Using the non-solvent induced phase separation (NIPS) method [34]. A homogeneous polymer solution was first prepared by dissolving PSF in NMP at the specified weight ratio, under continuous stirring at room temperature until the PSF pellets were completely dissolved. Then, the required amount of MMT powder was added and dispersed under stirring at 400 rpm for at least 6 hours, until a visually uniform suspension was attained. The casting solution was evenly spread onto a clean glass plate using a manual casting knife set at a thickness of 250 µm. The cast film was exposed to air for 20 seconds before being immersed in a coagulation bath containing distilled water at 25 °C. The glass plate was kept in the bath for 10 minutes to ensure complete phase inversion. The membranes obtained were thoroughly rinsed with deionized water multiple times to remove residual solvent and then dried at room temperature. Finally, they were stored in fresh distilled water before use. The compositions of PSF, NMP, and MMT are summarized in Table 1. Representative photos of the prepared membranes are shown in Figure 1.

Table 1. Membrane PSF-MMT composition.

Samples (wt%)	PSF (wt%)	MMT (wt%)	NMP
Neat PSF	13	0	87.0
M_1 (MMT-0.5%wt)	13	0.5	86.5
M_2 (MMT-1%wt)	13	1	86.0
M_3 (MMT-1.5%wt)	13	1.5	85.5
M_4 (MMT-2%wt)	13	2	85.0
M_5 (MMT-2.5%wt)	13	2.5	84.5

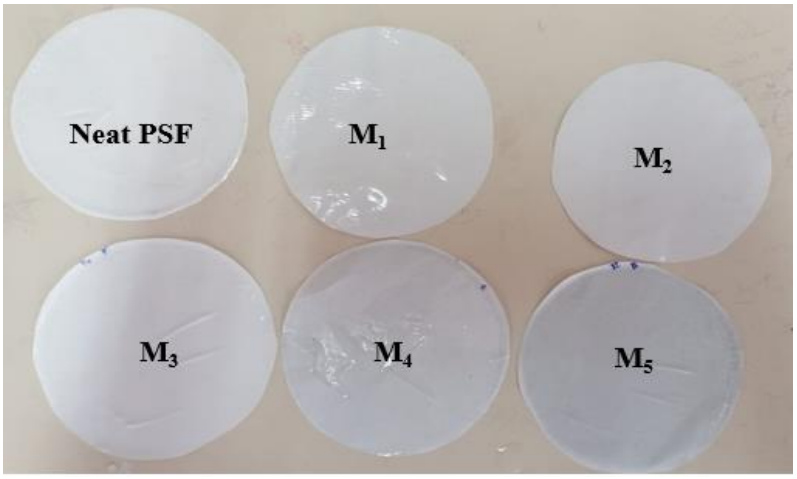

 doi:10.20944/preprints202510.1117.v1

Figure 1. Image of the different prepared membranes.

2.3. Characterization Techniques

Structural characterization of MMT powder and the prepared membranes was carried out with an X-ray diffractometer (Rigaku MiniFlex 600, Japan) equipped with CuKα radiation (λ = 1.5406 Å) operated at 40 kV and 20 mA. Powdered samples were scanned in the 2θ range of 5°–50°, with a step size of 0.02° and a scanning rate of 1°.min^{-1}.

Functional groups present on the powder and the different membranes were investigated using Fourier transform infrared spectroscopy (Spectrum Two FT-IR Spectrometer, Perkin-Elmer).

The surface (top-view) and cross-sectional morphologies of the membranes were examined using a field-emission scanning electron microscope (FE-SEM, ZEISS Cross Beam 350, Germany, S/N-8405010133). Cross-sections were prepared by immersing the membranes in liquid nitrogen and then fracturing them to preserve the original structure. To prevent charging during SEM observation, the samples were sputter-coated with a thin layer of platinum. Energy-dispersive X-ray spectroscopy (EDS) with an accelerating voltage of 15 kV, performed on a ZEISS Crossbeam 350 UHR-SEM instrument.

The surface hydrophilicity of the membranes was assessed using static water contact angle measurements. All samples were dried in an oven at 50 °C for 4 hours before testing. Measurements were performed with a CAM 200 Optical Contact Angle Meter at five different points on each membrane surface. For each sample, 4 measurements were performed, and both the average value and the standard deviation were calculated.

The mechanical strength of the membranes was characterized using a universal testing machine (Zwick/Roell, BTC-FR2. 5TN.D09, Germany). Tests were performed at 25 °C with a tensile speed of 10 mm.min^{-1} and a clamping distance of 25 mm. For each membrane type, a minimum of five measurements was conducted to ensure reproducibility and reduce experimental variability.

To examine the effect of MMT on membrane structure, porosity was measured using the gravimetric method. First, the membranes were dried at 50 °C for 24 hours. They were then cut into small pieces (1 cm × 1 cm), with five pieces prepared for each membrane, and their dry weights were recorded. The samples were then immersed in distilled water at 25 °C for 24 hours. After removing surface water with a paper filter, the wet weight of each piece was measured. The average dry and wet weights for each membrane were used to calculate porosity (ε) according to Equation 1 [35].

$$\varepsilon(\%) = \frac{\dfrac{W_1 - W_2}{\rho_w}}{\dfrac{W_1 - W_2}{\rho_w} + \dfrac{W_2}{\rho_m}} \times 100 \quad (1)$$

Where W_1 and W_2 are respectively the wet and dry weights of the membrane (g). ρ_w is the density of distilled water (0.998 g.mL^{-1} at 25 °C), and ρ_m is the density of the polymer (1.24 g.mL^{-1} at 25 °C).

The average pore radius (r_m) of the membranes was estimated using the Guerout–Elford–Ferry Equation 2 [36].

$$r_m = \sqrt{\frac{(2.9 - 1.75\,\varepsilon) \times 8\eta l Q}{\varepsilon A \Delta P}} \quad (2)$$

Where rm is the mean pore radius (m), η is the water viscosity (8.9 × 10^{-4} Pa.s), l is the membrane thickness (m) measured using a micrometer, Q is the volume of permeate water per unit time (m^3.s^{-1}), A is the effective area of the membrane (m^2), and ΔP is the operating pressure (Pa).

The chemical stability of the synthesized membranes was assessed by tracking their weight loss over time. Membrane samples were soaked in acidic (nitric acid, HNO_3, 0.2 M, pH=2) and alkaline (sodium hydroxide, NaOH, 0.5 M, pH=12) solutions at room temperature for three days. The weight

 doi:10.20944/preprints202510.1117.v1

of each membrane was measured at regular intervals to detect any degradation or chemical damage caused by the media.

2.4. Filtration Tests

The permeation tests were carried out using a cross-flow filtration system (see Figure 2). Before the tests, the membranes were compacted by circulation of distilled water at a trans-membrane pressure of 10-20 bar for 2 hours. This was carried out to reduce any effect on the membrane structure during the tests due to the pressure to which they are subjected to reach the steady flux. Experiments were performed in cross-flow filtration mode at 25° C at different trans-membrane pressure values (ΔP=10-20 bar). The pure water flux for each membrane was calculated using Equation 3 [37]:

$$J = \frac{V}{A \times t} \tag{3}$$

Where J is the permeating flux through the membrane, V is the permeate volume collected during the time t, and A is the membrane area (effective membrane area: 15.2 cm^2). The permeability was determined by plotting the slope of the flux versus the ΔP. Subsequently, an aqueous solution of DCF was prepared in distilled water at a concentration of 20 $mg.L^{-1}$ under 20 bar and 25 °C.

The permeate was collected every 10 min, and the quantitative determination of the drug was carried out using a UV spectrophotometer (UV–3100 PC Spectrophotometer, China) at a wavelength of 273 nm. The rejection was calculated as follows [38]:

$$R(\%) = \frac{C_i - C_f}{C_i} \times 100 \tag{4}$$

Where C_i and C_f are the concentrations of the drug ($mg.L^{-1}$) in permeate and feed, respectively.

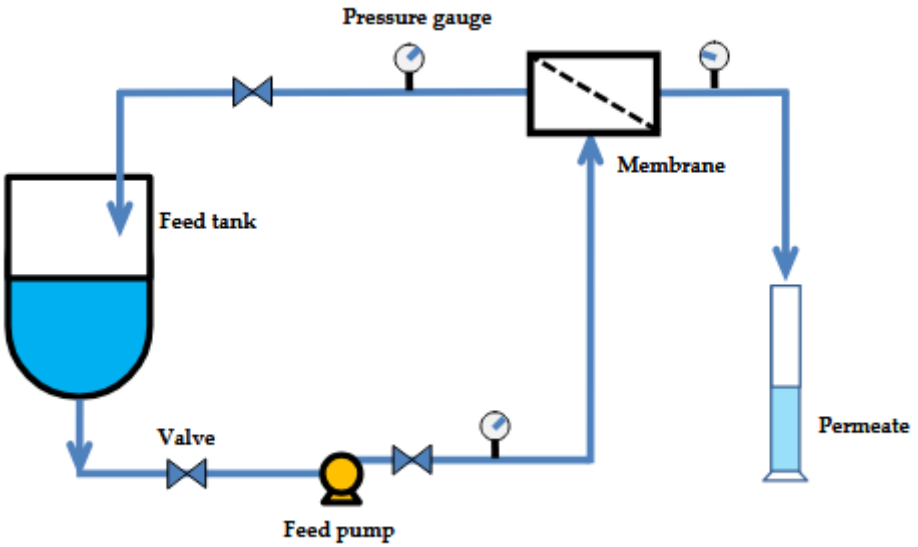

Figure 2. Schematic diagram of the cross-flow filtration unit used.

2.5. Fouling Studies Test

The flux recovery ratio (FRR) quantifies the ability of the membrane to recover its permeability after filtration and cleaning. In this case, the antifouling performance of the membrane was evaluated using a bovine serum albumin (BSA) solution (50 $mg.L^{-1}$). The process involved three main steps:

- Pure water filtration at 20 bar to obtain the initial pure water flux (J_w).
- BSA solution filtration,

 doi:10.20944/preprints202510.1117.v1

- Cleaning the membrane with distilled water to remove reversible foulants, followed by measuring the recovered pure water flux (J_{wa}).

The FRR of the membrane was then estimated using equation (5) [31,39]:

$$FRR(\%) = \frac{J_{wa}}{J_w} \times 100 \quad (5)$$

3. Results and Discussion

3.1. Characterization of Montmorillonite (MMT)

The XRD pattern of MMT clay (Figure 3) shows a strong reflection at 2θ = 9.9°, corresponding to the (001) basal plane with an interlayer spacing of approximately 8.8 Å. This spacing is slightly smaller than the typical hydrated montmorillonite value (12–15 Å), indicating a partially dehydrated or collapsed structure [40]. Additional reflections at higher angles, such as 20°, 22°, 35°, and 62°, can be attributed to higher-order reflections as well as the presence of crystalline impurities, mainly quartz and feldspar, that are commonly associated with natural clays. Moreover, the broad background hump between 20° and 35° suggests the presence of partially amorphous phases or structural disorder within the clay [41]. Overall, the diffraction profile confirms the crystalline fingerprint of montmorillonite, reflecting both its ordered layered structure and the contribution of minor impurities and amorphous components.

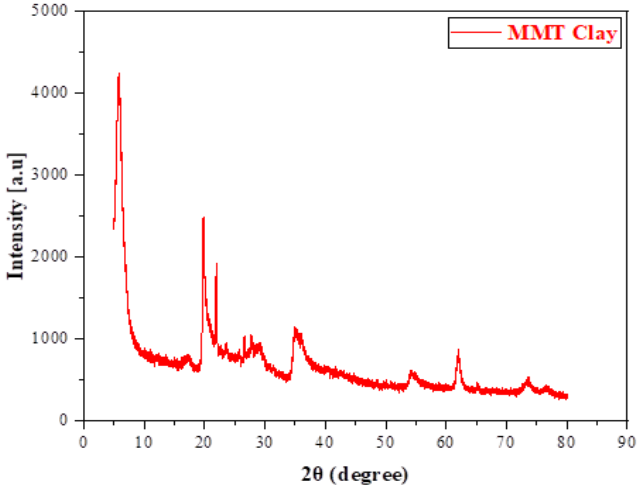

Figure 3. XRD patterns of montmorillonite (MMT) clay.

The FTIR spectrum of MMT clay, shown in Figure 4, displays characteristic vibrational bands linked to its layered silicate structure. The broad absorption peaks at 3630 cm^{-1} and 3387 cm^{-1} are assigned to O–H stretching vibrations from structural hydroxyl groups and adsorbed water molecules, respectively [42]. A distinct band at 1642 cm^{-1} is attributed to the bending vibrations of water molecules in the interlayer spaces [43]. In the lower wavenumber region (1200–400 cm^{-1}), the strong absorption at 1120 cm^{-1} corresponds to the Si–O stretching vibration of tetrahedral silicate sheets, while the peak at 997 cm^{-1} relates to the in-plane Si–O stretching mode, confirming the integrity of the layered silicate framework [44]. Peaks at 789 cm^{-1} and 695 cm^{-1} are linked to Al–Mg–OH and Al–OH bending vibrations, respectively [45]. The low-wavenumber band around 524 cm^{-1} is assigned to Si–O–Al bending modes. Overall, the FTIR profile verifies the typical structural features of montmorillonite clay, indicating its preserved layered structure with characteristic hydroxyl and silicate functionalities, as reported in previous studies [43,45].

 doi:10.20944/preprints202510.1117.v1

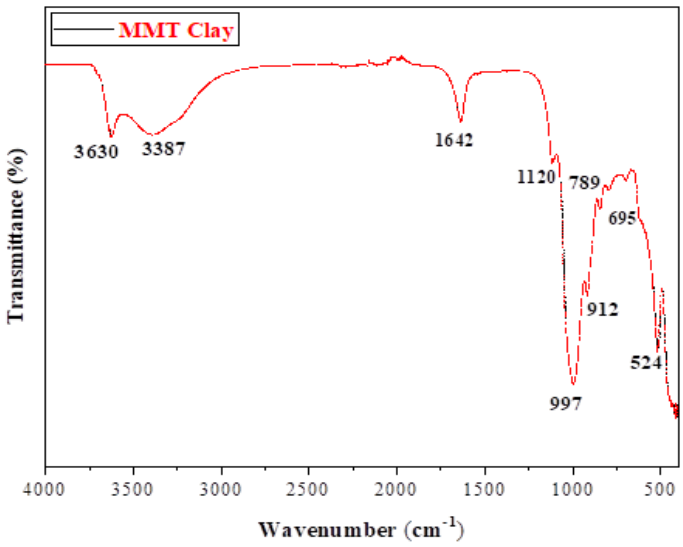

Figure 4. FT-IR spectrum of montmorillonite (MMT) clay.

3.2. Membrane Characterization

3.2.1. XRD Analysis

To investigate the structural properties and verify the successful incorporation of montmorillonite (MMT) clay into the polysulfone (PSF) matrix, X-ray diffraction (XRD) analyses were performed on the pristine and mixed matrix membranes, as shown in Figure 5.

The diffraction pattern of neat PSF shows a broad amorphous halo, characteristic of its non-crystalline structure. When MMT is incorporated at different loadings, noticeable changes appear in the diffraction profiles. At low clay concentrations (M_1 and M_2), the disappearance or broadening of the characteristic basal reflection of MMT indicates exfoliation and/or intercalation of silicate layers within the PSf matrix. This suggests good dispersion of the clay, with polymer chains penetrating between clay platelets.

As the MMT content increases (M_3–M_5), the intensity of certain reflections becomes more pronounced, indicating the partial restacking or aggregation of clay platelets at higher loadings. However, the overall amorphous nature of PSf is preserved, confirming that no significant crystalline domains are formed.

These findings show that MMT was successfully integrated into the PSF matrix, with mostly exfoliated and intercalated structures at low loadings, while higher concentrations tend to cause partial aggregation. These structural changes are likely to affect the physical and functional properties of the membranes, including their hydrophilicity, permeability, and mechanical strength [43,46].

 doi:10.20944/preprints202510.1117.v1

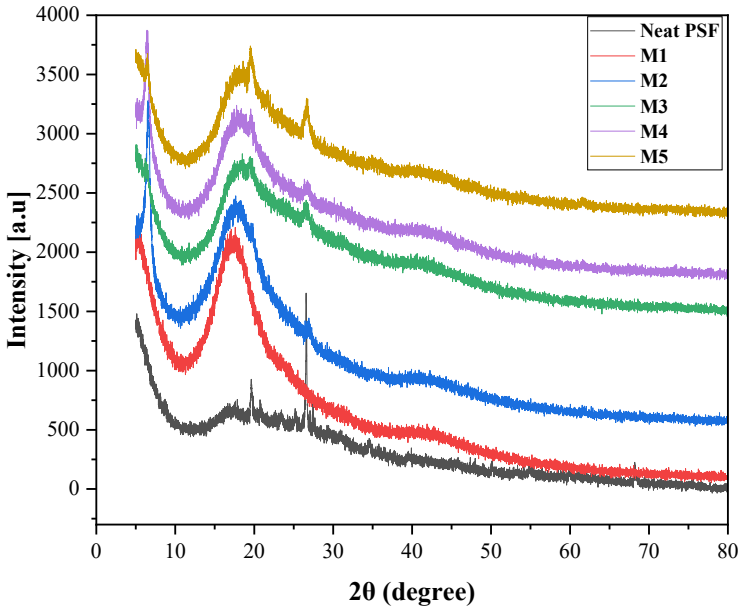

Figure 5. XRD pattern of pristine and mixed matrix membranes: M_1 (PSF/MMT-0.5%), M_2 (PSF/MMT-1%), M_3 (PSF/MMT-1.5%), M_4 (PSF/MMT-2%) and M_5 (PSF/MMT-2.5%).

3.2.2. FT-IR Studies

Figure 6 displays the FTIR spectra of the pristine polysulfone (PSF) membrane and the PSF–MMT membranes. The spectrum of pristine PSF exhibits the characteristic bands of the polymer: aromatic C–H stretching at 3100–3000 cm^{-1}, aliphatic C–H stretching at 2920 cm^{-1}, aromatic C=C vibrations around 1585 cm^{-1}, and the strong sulfone (S=O) absorptions at 1320–1290 cm^{-1} (asymmetric) and 1150–1130 cm^{-1} (symmetric). In addition, the ether (C–O–C) stretching band is observed near 1240 cm^{-1}, confirming the polysulfone backbone [47]. After the incorporation of montmorillonite, new peaks appeared: a broad absorption in the 3200–3600 cm^{-1} region, associated with surface hydroxyl groups and interlayer water of the clay (M_3, M_4, and M_5), and a strong band in the 1000–1100 cm^{-1} region, attributed to Si–O stretching vibrations of the silicate layers [48]. Slight broadening and shifts of the characteristic PSF bands, especially those corresponding to S=O and C–O–C, indicate interfacial interactions (hydrogen bonding and ion–dipole contacts) between the oxygen-containing groups of PSF and the hydroxyl sites of MMT [49]. As shown in Figure 6, the absence of new functional bands suggests that MMT incorporation occurs mainly through physical interactions rather than covalent bonding, which is consistent with a previous paper that reports on PSf–MMT hybrid membranes [50].

 doi:10.20944/preprints202510.1117.v1

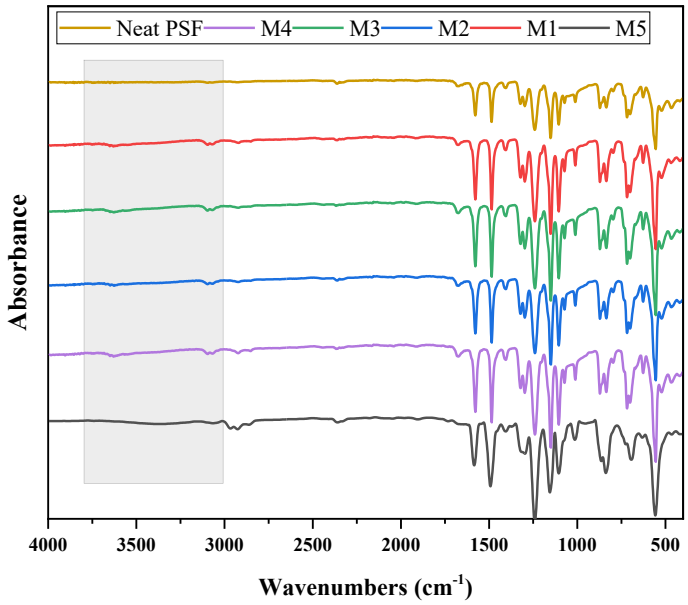

Figure 6. FT-IR spectra of the different prepared membranes.

3.2.3. Morphological Studies

The surface and cross-section morphologies of the prepared membranes were examined using SEM (see Figure 7). All membranes displayed a characteristic asymmetrical structure, with a dense top layer and a porous sublayer (see Figure 7). The pristine membrane had a smooth, compact surface with limited porosity and an asymmetric cross-section featuring finger-like macrovoids, as shown in Figure 7. Membranes M_1 and M_2 developed surface pores along with larger, more prominent finger-like structures. Among all samples, M_3 showed the highest surface porosity, with well-connected macrovoids, indicating rapid phase inversion during fabrication. Its surface morphology exhibited uniformly distributed circular pores, suggesting improved permeability potential. In contrast, M_4 and M_5 demonstrated moderate porosity and relatively denser structures. Notably, M_5 features a thin skin layer covering the finger-like substructure. Overall, these morphological improvements, especially in M_2 and M_3, are likely to enhance membrane performance, particularly for high-flux and selective separation applications.

Elemental microanalysis using Energy Dispersive X-ray Spectroscopy (EDS) was carried out to analyze the elemental composition of the polysulfone (PSf) and mixed matrix membranes. The EDS spectra and corresponding SEM images (Figure 8) reveal the presence and distribution of key elements: carbon (C), oxygen (O), and silicon (Si). The neat PSf membrane showed a high carbon content (64.7 wt%) and a significant oxygen level (20.7 wt%), typical of its aromatic and sulfone backbone. As expected, no silicon was detected in the neat membrane, confirming its unmodified state.

The MMMs displayed silicon content (ranging from 1.1 to 1.4 wt%). These results demonstrate successful incorporation of silicon-based additives into the membrane matrix. The presence of silicon in these samples provides direct evidence of surface modification and suggests potential improvements in membrane hydrophilicity, fouling resistance, and mechanical stability (see Figure 8).

EDS analysis confirmed successful chemical modification of the PSF membranes with MMT, which corresponded to SEM-observed morphological changes. Modified membranes exhibited more pronounced finger-like pores and increased macrovoid formation, likely enhancing water permeability and overall functional performance in future evaluations.

 doi:10.20944/preprints202510.1117.v1

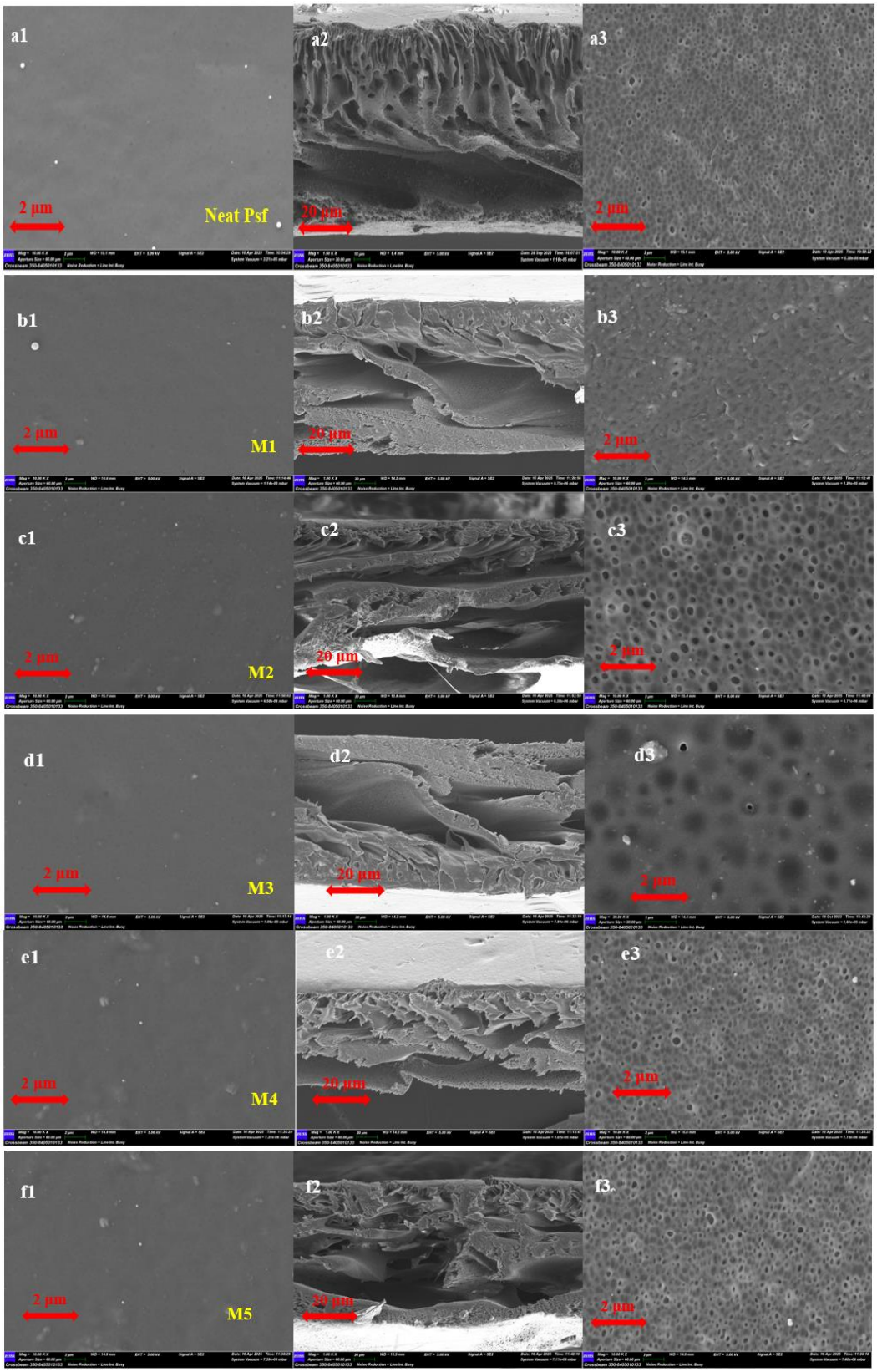

Figure 7. Top surface and cross-section SEM images of PSF-MMT membranes prepared with different compositions of MMT, (Neat PSF), M_1 (with 0.5 wt% of MMT),) M_2 (with 1 wt% of MMT), M_3 (with 1.5 wt% of MMT), M_4 (with 2 wt% of MMT), and M_5 (with 2.5 wt% of MMT). 1: Top surface; 2: Cross section; 3: Bottom section.

 doi:10.20944/preprints202510.1117.v1

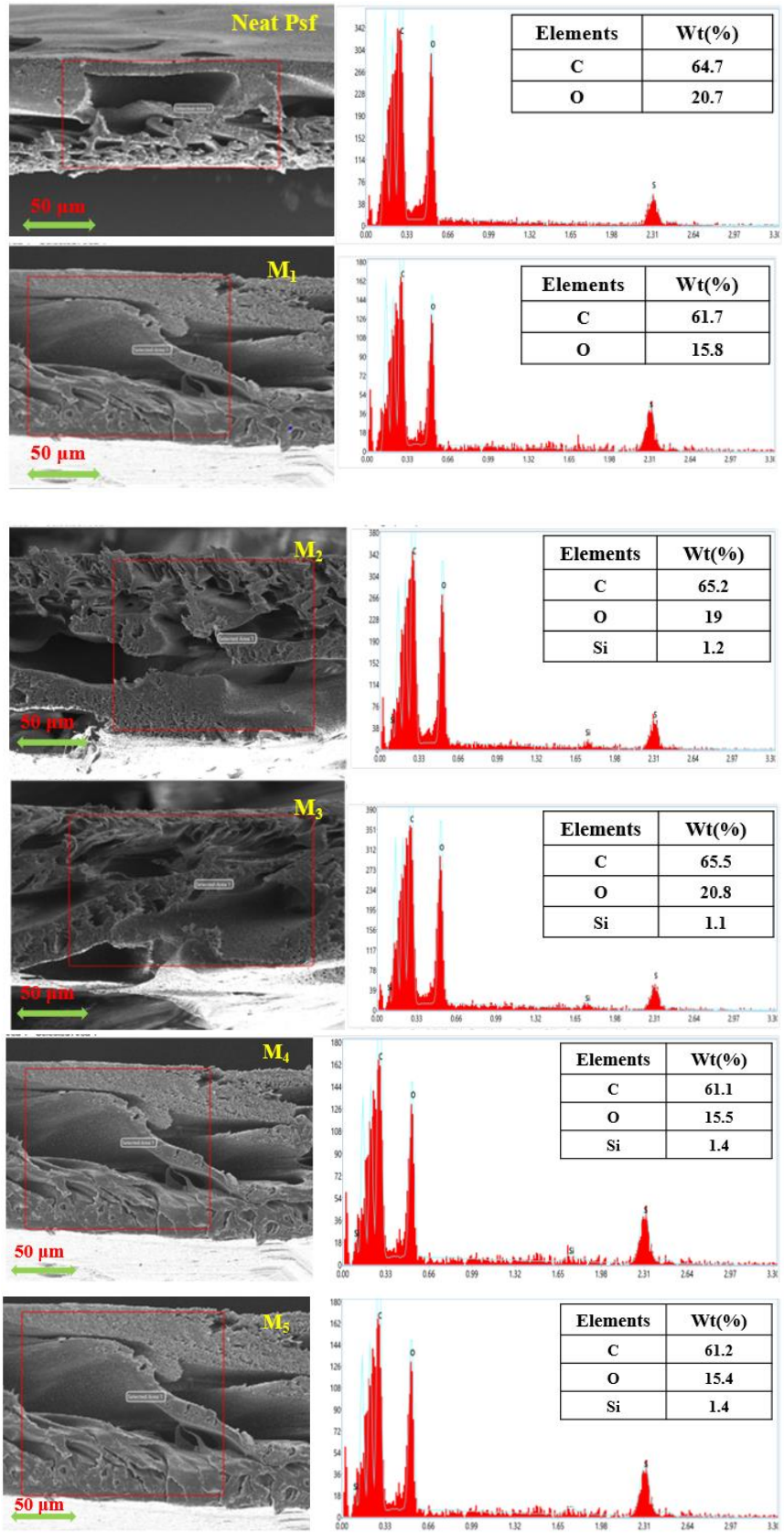

Figure 8. Elemental microanalyses and EDS pattern of the different samples: Neat PSF, M_1(MMT-0.5%wt), M_2(MMT-1%wt), M_3(MMT-1.5%wt), M_4(MMT-2%wt), and M_5(MMT-2.5%wt).

 doi:10.20944/preprints202510.1117.v1

Table 1. Effect of MMT content on Tensile strength (MPa), Tensile Strain at Break (%), and Young's modulus of the different prepared membranes.

Membrane's types	Tensile Strain at Break (%)	Tensile Strength (MPa)	Young's Module (MPa)
Neat PSF	21.73 ± 1.18	3.97 ± 1.00	93.65 ± 1.04
M_1 (MMT-0.5%wt)	29.43 ± 1.02	4.47 ± 1.05	70.08 ± 1.20
M_2 (MMT-1%wt)	30.91 ± 1.17	3.61 ± 1.08	106 ± 1.02
M_3 (MMT-1.5%wt)	37.45 ±1.35	3.44 ± 1.11	97.64 ± 1.02
M_4 (MMT-2%wt)	38.40 ±1.20	3.80 ± 1.05	94.52 ± 1.16
M_5 (MMT-2.5%wt)	35.95 ±1.08	3.50 ± 1.05	91.62 ± 1.05

The addition of MMT improved the mechanical flexibility of the membranes, with tensile strain at break rising from 21.73% for the neat PSF membrane to a maximum of 38.4% for M4. This enhancement is due to the reinforcing effect and good dispersion of MMT clay within the polymer matrix [51]. Although tensile strength remained relatively stable across different formulations, the highest value (4.47 MPa) was observed at low MMT content (M_1), indicating effective stress transfer at lower filler levels [52]. Young's modulus varied with composition, with M_2 exhibiting the highest stiffness (106 MPa), indicating enhanced rigidity at moderate MMT loading. Additionally, an increase in the clay content to 2.5 wt.% led to a decline in mechanical properties, likely due to particle aggregation and poor dispersion. These results suggest that optimal MMT incorporation can simultaneously improve the ductility and mechanical strength of the membranes.

Table 2. Mean pore size and porosity of the PSF-MMT membranes.

Membrane's types	Mean Pore radius r (nm)	Porosity (%)
Neat PSF	16.7 ± 0.6	74
M_1 (MMT-0.5%wt)	18.9 ± 0.4	80
M_2 (MMT-1%wt)	22.4 ± 0.8	86
M_3 (MMT-1.5%wt)	24.4 ± 0.5	89
M_4 (MMT-2%wt)	19.0 ± 0.7	82
M_5 (MMT-2.5%wt)	21.0 ± 0.6	85

Porosity and SEM analyses highlight the significant influence of montmorillonite (MMT) on the structure and performance of PSF membranes. With MMT addition, both the mean pore radius and overall porosity increased, likely due to the hydrophilic nature of the clay accelerating solvent–nonsolvent exchange during phase inversion. SEM images confirmed that membranes M_3 exhibited the largest and most uniform pores, corresponding to enhanced water transport and reduced fouling [51]. However, when the MMT content exceeded 1.5 wt%, particle agglomeration occurred. These aggregates reduced the effective surface area and partially blocked the membrane pores, as observed in M_4 and M_5 membranes. Consequently, the pore radius and overall porosity decreased, and the membranes exhibited a higher contact angle, indicating reduced hydrophilicity [20]. Despite these limitations at high loadings, SEM micrographs still revealed a relatively well-dispersed porous network, demonstrating that careful control of MMT concentration is critical to optimizing both morphology and functional performance. Overall, these findings show that MMT incorporation can significantly improve membrane structure and water transport properties, provided aggregation is avoided [53].

 doi:10.20944/preprints202510.1117.v1

3.2.4. Chemical Resistance

Chemical cleaning of membranes is an accepted method to reduce flux decline and fouling. Among various cleaning techniques, chemical cleaning is the most common.. Acidic agents are used to remove inorganic contaminants, while alkaline agents target organic contaminants, including microorganisms. However, chemical cleaning can significantly impact the physical and chemical properties of the membrane causing surface damage and loss of selectivity. Therefore, chemical resistance in acidic and alkaline conditions was assessed. The percentage of weight loss over time is shown in Figure 9. After three days (72 hours), the weight loss ranged from 0.25% to 2.5% across the different membranes. Among the tested samples, the M_2 membrane exhibited the highest stability in alkaline solution, whereas the M_4 membrane showed superior resistance in acidic medium.

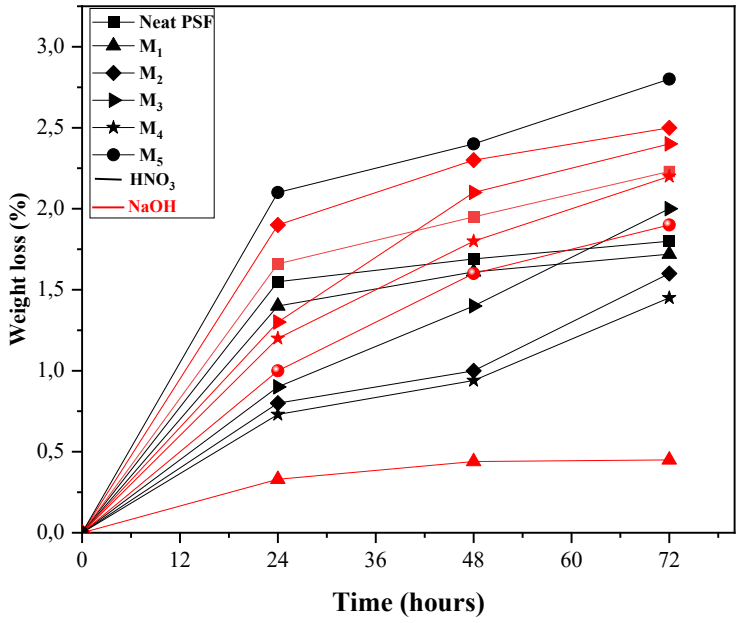

Figure 9. Weight loss percentage versus time of the prepared membranes after immersion in HNO_3 and NaOH for 3 days at room temperature.

3.2.5. Hydrophilicity and Water Permeability

Hydrophilic membranes are commonly used in wastewater treatment because they have higher water flux and are less prone to fouling [54]. Adding montmorillonite (MMT) into the PSF matrix greatly increased the surface hydrophilicity of the membranes, as shown by static water contact angle measurements (Figure 10). The pure PSF membrane showed a contact angle of 83°, reflecting its hydrophobic character. Incorporation of MMT progressively reduced the contact angle, reaching 57° for membrane M_5, indicating enhanced hydrophilicity.

This effect is attributed to the migration of MMT clay to the membrane surface during phase inversion. This migration, driven by exposure to water (the non-solvent), is facilitated by the hydrophilic nature and negative surface charge of MMT [55]. This process, commonly referred to as "fining," leads to the accumulation of MMT at the water–membrane interface, enhancing surface wettability. Consequently, the increased hydrophilicity results in a significant improvement in pure water permeability.

The water permeability of the unmodified PSF membrane was 4 $L.m^{-2}.h^{-1}.bar^{-1}$, whereas the M_5 membrane exhibited the highest permeability at 21.33 $L.m^{-2}.h^{-1}.bar^{-1}$. This trend was consistent across all modified membranes (M_1–M_5), underscoring the beneficial effect of MMT on both surface properties and water transport efficiency.

 doi:10.20944/preprints202510.1117.v1

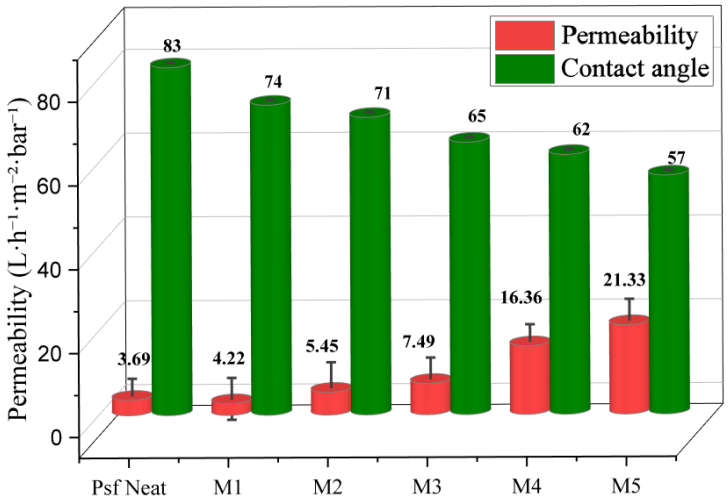

Figure 10. Pure water permeability and static contact angle of the MMT-PSF membranes.

3.3. Application on DCF Removal, BSA Rejection, and Antifouling Properties

The influence of montmorillonite (MMT) incorporation into polysulfone (PSF) membranes on diclofenac (DCF) and bovine serum albumin (BSA) removal efficiencies, as well as on the flux recovery ratio (FRR), is illustrated in Figure 11.

All experiments were conducted under controlled operating conditions: a transmembrane pressure of 20 bar, pH 7 ± 0.2, an initial diclofenac (DCF) concentration of 20 mg.L^{-1}, and a feed temperature of 25 ± 0.5 °C. The pristine PSF membrane showed modest performance, achieving 10% DCF removal, 49% BSA rejection, and 71% FRR.

The incorporation of MMT led to a significant improvement in the membrane performance. Specifically, DCF removal gradually increased with MMT loading, reaching a maximum of 79% for membrane M_4. This improvement is due to the higher hydrophilicity and additional adsorption sites provided by MMT, which enhance the interactions between DCF molecules and the membrane matrix. However, at higher loading (membrane M_5), DCF removal dropped to 51.2%, probably because MMT agglomeration disrupted membrane structure and lowered separation efficiency.

Similarly, BSA rejection increased from 49% (neat PSF) to 89% for membranes M_3 and M_4, reflecting a tighter membrane structure and improved size exclusion capabilities. This improvement is likely due to well-dispersed MMT particles modifying the pore structure and reducing macrovoids formation. A slight decrease to 88% for M_5 suggests that excessive filler content can compromise structural uniformity [56].

The antifouling performance, as indicated by the FRR, also showed significant improvement. FRR increases from 71% for the neat PSf membrane to 89% for M_3 and remained high at 82% for both M_4 and M_5. The enhanced antifouling behavior is due to the increase of hydrophilicity and a smoother surface morphology provided by the MMT, which decreases foulant adhesion and improves membrane cleanability [57].

Overall, membrane M4 demonstrated the most balanced performance by achieving high DCF removal (79%), excellent BSA rejection (89%), and strong antifouling properties (FRR = 82%). These results indicate that there is an optimal level of MMT loading, as excessive amounts could lead to negative morphological changes that diminish the benefits of MMT addition.

 doi:10.20944/preprints202510.1117.v1

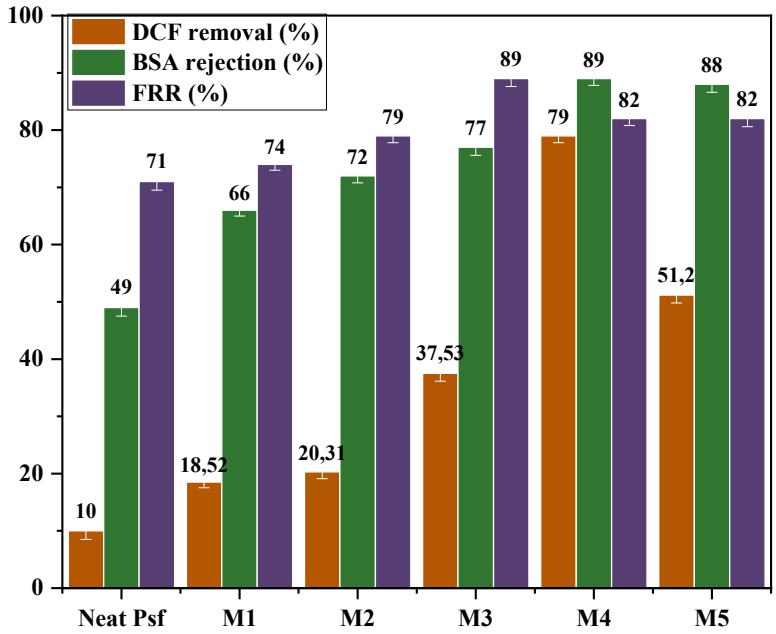

Figure 11. Diclofenac, BSA rejection, and antifouling FRR of the PSF membrane with various MMT contents. (Operating pressure =10 bar, pH = 7 ± 0.2, Initial DCF concentration = 20 mg.L^{-1}, feed temperature = 25 °C).

3.4. Diclofenac (DCF) Removal Mechanism by PSF/MMT Composite Membranes

The removal mechanism of diclofenac (DCF) using mixed matrix membranes (MMMs) based on polysulfone incorporating montmorillonite (MMT) involves a synergistic combination of physical and physicochemical processes. Initially, DCF in aqueous solution—mainly in its ionized form (carboxylate anions at neutral pH)—is partially retained through physical sieving as it passes through the membrane pores. This filtration is governed by the molecular size of DCF (296 Da) and the microporous structure of the membrane, which is enhanced by the presence of MMT.

In addition to this mechanical retention, a significant portion of DCF is removed through specific adsorption onto the layered structure of MMT. Montmorillonite provides a high specific surface area and abundant surface functional groups (–OH, Al–OH, Si–O–Si) that enable multiple interaction mechanisms with DCF molecules. These include hydrogen bonding between the carboxylic or amine groups of DCF and the hydroxyl sites of MMT, electrostatic interactions between negatively charged DCF species and the polar regions of the clay, and π–π stacking between the aromatic rings of DCF and the silicate layers of MMT. Such synergistic interactions result in strong binding of DCF molecules at the clay–polymer interface.

Moreover, the lamellar structure of MMT acts as a molecular trap, effectively immobilizing DCF within the membrane matrix [58]. This dual mechanism of filtration and adsorption is further promoted by the increased hydrophilicity of the membrane resulting from MMT incorporation, which enhances its affinity toward polar organic compounds such as DCF. Consequently, PSF/MMT membranes achieve a high DCF removal efficiency (up to 79%) while maintaining excellent water permeability and antifouling resistance.

As shown in Figure 12, electrostatic attraction between DCF anions and the polar hydroxyl sites of MMT, combined with hydrophobic π–π stacking, facilitates strong immobilization of DCF molecules within the membrane matrix.

 doi:10.20944/preprints202510.1117.v1

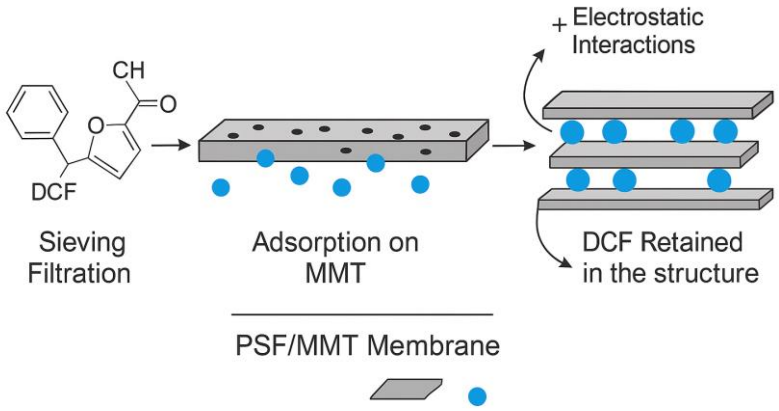

Figure 12. *Schematic representation of the diclofenac (DCF) removal mechanism by PSF/MMT composite membranes.*

4. Comparative Analysis of Literature Data for DCF Removal Using PSF-Based Membranes

Table 3 presents a comparison of various polymeric and mixed matrix membranes (MMMs) prepared by the phase inversion method for diclofenac (DCF) removal. In a recent study, we developed a PSF–GO nanocomposite membrane (PSF: 13 wt%, GO: 0.5 wt%, NMP: 86.5 wt%). This membrane exhibited a flux of 7.2 $L.m^{-2}.h^{-1}.bar^{-1}$ and achieved a high DCF removal efficiency of 78.5%, which is superior to most reported PSF-based membranes. The enhanced performance is attributed to the incorporation of GO, which significantly improved the hydrophilicity, surface activity, and antifouling properties of the membrane [19].

In comparison, the PSF–MC/AC (0.5) membrane reported by Nadour et al. [59] exhibited a higher flux (17.5 $L.m^{-2}.h^{-1}.bar^{-1}$) but lower removal efficiency (44.7%), due to the limited interaction of activated carbon with DCF in aqueous matrices. The PSF–PVA membrane exhibited a moderate removal efficiency (60%) and loose nanofiltration behavior, accompanied by a higher tendency to foul, despite its ability to be chemically regenerated using NaOH [60]. Similarly, the PSF–MMT membrane achieved a removal efficiency of 79% which can be attributed to the improved membrane structure resulting from the incorporation of montmorillonite, enhancing both hydrophilicity and adsorption capacity.

Overall, the developed PSF–MMT membranes demonstrate a favorable balance between high contaminant removal, adequate permeation flux, and resistance to fouling, underscoring their potential for practical application in the treatment of pharmaceutical wastewater.

Table 3. Comparative Analysis of Literature Data for DCF Removal using PSF-Based Membranes.

Membrane Composition / Additive	Composition of Membrane (weight % of each material)	Operating Conditions (TMP, Feed Conc., pH, etc.)	Permeability / Flux ($L.m^{-2}.h^{-1}.bar^{-1}$)	DCF Removal (%)	Notes / Fouling & Regeneration	References
PSF + GO nanocomposite	PSF: 13%wt; GO: 0.5%wt; NMP: 86.5%wt	TMP: 20 bar; Feed Conc.: 12 $mg.L^{-1}$; pH: 7.5	7.2	78.5	Improved hydrophilicity; Flux and DCF removal.	[59]
PSF-MC (0.5)-AC (0.5) (Methylcellulose activated carbon)	PSF: 13%wt; AC: 0.5%wt; MC: 0.5%wt; NMP: 86%wt	TMP: 1 bar; Feed Conc.: 10 $mg.L^{-1}$	17.5	44.68	The incorporation of activated carbon into the membrane matrix increased the Young's modulus to	[16]

 doi:10.20944/preprints202510.1117.v1

					136.2 MPa, thereby enhancing the membrane's rigidity.	
PSF + PVA	PSF: 80%; PVA: 20%	TMP: 1 bar; Feed Conc.: 2 $mg.L^{-1}$; pH: 6	20	60	Loose NF behavior; moderate fouling; regeneration with NaOH.	[60]
PSF + MMT	PSF:13 **(wt%)**; MMT:2.5 **(wt%), NMP:** 84.5(wt%),	TMP: 20 bar; Feed Conc.: 20 $mg.L^{-1}$; pH: 7	7.5	79	Good antifouling performance (FRR = 82%); high DCF removal despite high feed concentration; moderate flux.	Present studies

Notes: PSF: Polysulfone; **GO**: Graphene Oxide; **PVA**: Polyvinyl Alcohol; **MC:** Methylcellulose; **AC**: Activated Carbon; **ZnO**: Zinc Oxide; **NaOH**: Sodium Hydroxide.

5. Conclusion

This study demonstrated that incorporating montmorillonite (MMT) into polysulfone (PSF) membranes significantly enhances their performance in water treatment, particularly for the removal of pharmaceutical contaminants such as diclofenac (DCF). At the optimal MMT loading of 2 wt%, the composite membranes exhibited improved water permeability (7.5 $L.m^{-2}.h^{-1}.bar^{-1}$), effective DCF removal (79%), and excellent antifouling properties. When tested with bovine serum albumin (BSA) as a model foulant, the M4 membrane achieved a high rejection rate (89%) and a flux recovery ratio (FRR) exceeding 82%. However, at higher MMT concentrations (2.5 wt%), particle aggregation occurred, adversely affecting permeability, rejection, and fouling resistance. These findings highlight the importance of optimizing the filler content to achieve a balanced combination of flux, selectivity, and structural stability.

Overall, PSF/MMT nanocomposite membranes show strong potential for advanced water purification applications, offering a durable and efficient approach for mitigating pharmaceutical pollutants in wastewater. Future work will focus on scaling up the PSF/MMT system for continuous-flow applications and testing with real pharmaceutical wastewater.

Acknowledgments: The authors gratefully acknowledge funding from the TRUST Prima program (research project supported by the European Commission).

Author Contributions: Conceptualization, Lasâad DAMMAK and Raja BEN AMAR; **Data curation**, Zouhair SALAH and Hajer ALOULOU; **Investigation**, Zouhair SALAH, Hajer ALOULOU, Catia ALGIERI, Lasâad DAMMAK and Raja BEN AMAR; Methodology, Zouhair SALAH and Hajer ALOULOU; Project administration, Raja BEN AMAR; Software, Zouhair SALAH, Hajer ALOULOU, Catia ALGIERI; **Supervision**, Lasâad DAMMAK and Raja BEN AMAR; Validation, Catia ALGIERI, Lasâad DAMMAK and Raja BEN AMAR; Writing – original draft, Zouhair SALAH and Hajer ALOULOU; Writing – review & editing, Catia ALGIERI and Raja BEN AMAR.

Funding: This work has received funding from the PRIMA Foundation. Grant Agreement number: [2024] [TRUST]-Call 2020 Section 1 Water IA.

Institutional Review Board Statement: Not applicable.

Informed Consent Statement: Not applicable.

Data Availability Statement: The data presented in this study are available on request from the corresponding author.

Conflicts of Interest: The authors declare no conflicts of interest.

 doi:10.20944/preprints202510.1117.v1

References

1. Afshar, N.R.; Fahmi, H. Impact of Climate Change on Water Resources in Iran. *Int. J. Energy Water Resour.* **2019**, *3*, 55–60.
2. Abbott, B.W.; Bishop, K.; Zarnetske, J.P.; Hannah, D.M.; Frei, R.J.; Minaudo, C.; Chapin, F.S.; Krause, S.; Conner, L.; Ellison, D.; et al. A Water Cycle for the Anthropocene. *Hydrol. Process.* **2019**, *33*, 3046–3052, doi:10.1002/hyp.13544.
3. Akhil, D.; Lakshmi, D.; Kartik, A.; Vo, D.V.N.; Arun, J.; Gopinath, K.P. *Production, Characterization, Activation and Environmental Applications of Engineered Biochar: A Review*; Springer International Publishing, 2021; Vol. 19; ISBN 0123456789.
4. Hernando, M.D.; Mezcua, M.; Fern, A.R.; Barcel, D. Environmental Risk Assessment of Pharmaceutical Residues in Wastewater Effluents , Surface Waters and Sediments. **2006**, *69*, 334–342, doi:10.1016/j.talanta.2005.09.037.
5. Van Tran, T.; Nguyen, D.T.C.; Le, H.T.N.; Vo, D.-V.N.; Nanda, S.; Nguyen, T.D. Optimization, Equilibrium, Adsorption Behavior and Role of Surface Functional Groups on Graphene Oxide-Based Nanocomposite towards Diclofenac Drug. *J. Environ. Sci.* **2020**, *93*, 137–150.
6. de Franco, M.A.E.; de Carvalho, C.B.; Bonetto, M.M.; de Pelegrini Soares, R.; Féris, L.A. Diclofenac Removal from Water by Adsorption Using Activated Carbon in Batch Mode and Fixed-Bed Column: Isotherms, Thermodynamic Study and Breakthrough Curves Modeling. *J. Clean. Prod.* **2018**, *181*, 145–154.
7. Álvarez, S.; Ribeiro, R.S.; Gomes, H.T.; Sotelo, J.L.; García, J. Chemical Engineering Research and Design Synthesis of Carbon Xerogels and Their Application in Adsorption Studies of Caffeine and Diclofenac as Emerging Contaminants. *Chem. Eng. Res. Des.* **2014**, *95*, 229–238, doi:10.1016/j.cherd.2014.11.001.
8. Phasuphan, W.; Praphairaksit, N.; Imyim, A. Removal of Ibuprofen, Diclofenac, and Naproxen from Water Using Chitosan-Modified Waste Tire Crumb Rubber. *J. Mol. Liq.* **2019**, *294*, 111554, doi:10.1016/j.molliq.2019.111554.
9. Caban, M.; Lis, E.; Kumirska, J.; Stepnowski, P. Science of the Total Environment Determination of Pharmaceutical Residues in Drinking Water in Poland Using a New SPE-GC-MS (SIM) Method Based on Speedisk Extraction Disks and DIMETRIS Derivatization. *Sci. Total Environ.* **2015**, *538*, 402–411, doi:10.1016/j.scitotenv.2015.08.076.
10. Salah, Z.; Aloulou, H.; Bhattacharyya, S.; Algieri, C.; Amar, R. Ben Potential Elimination of Diclofenac Sodium (DCF) from Aqueous Solution by Adsorption Using Orange Peel Waste-Based Activated Carbon. *Euro-Mediterranean J. Environ. Integr.* **2025**, doi:10.1007/s41207-025-00822-1.
11. Beltrán, F.J.; Pocostales, P.; Alvarez, P.; Oropesa, A. Diclofenac Removal from Water with Ozone and Activated Carbon. **2009**, *163*, 768–776, doi:10.1016/j.jhazmat.2008.07.033.
12. José M. Angosto, M.J.R. and J.A.F.-L.* Removal of Diclofenac in Wastewater Using Biosorption and Advanced Oxidation Techniques : *Water* **2020**, *12*.
13. Mansouri, F.; Chouchene, K.; Roche, N.; Ksibi, M. Removal of Pharmaceuticals from Water by Adsorption and Advanced Oxidation Processes: State of the Art and Trends. *Appl. Sci.* **2021**, *11*, doi:10.3390/app11146659.
14. SLOBODA RIGOBELLO, E.; DI BERNARDO DANTAS, A.; DI BERNARDO, L.; VIEIRA, E.M. Removal of Diclofenac by Conventional Drinking Water Treatment Processes and Granular Activated Carbon Filtration. *Chemosph.* **2013**, *92*, 184–191.
15. Vergili, I. Application of Nanofiltration for the Removal of Carbamazepine, Diclofenac and Ibuprofen from Drinking Water Sources. *J. Environ. Manage.* **2013**, *127*, 177–187, doi:10.1016/j.jenvman.2013.04.036.
16. Nadour, M.; Boukraa, F.; Benaboura, A. Removal of Diclofenac , Paracetamol and Metronidazole Using a Carbon- Polymeric Membrane. *J. Environ. Chem. Eng.* **2019**, *7*, 103080, doi:10.1016/j.jece.2019.103080.
17. Martins, W.; Val, P.; Vieira, S.; Fernandes, M. Diclofenac Removal from Water by Adsorption on Moringa Oleifera Pods and Activated Carbon : Mechanism , Kinetic and Equilibrium Study On E. *J. Clean. Prod.* **2019**, *219*, 809–817, doi:10.1016/j.jclepro.2019.02.129.
18. Lai, G.S.; Lau, W.J.; Goh, P.S.; Ismail, A.F.; Yusof, N.; Tan, Y.H. Graphene Oxide Incorporated Thin Film Nanocomposite Nanofiltration Membrane for Enhanced Salt Removal Performance. *Desalination* **2016**, *387*, 14–24, doi:10.1016/j.desal.2016.03.007.

19. Salah, Z.; Bhattacharyya, S.; Cozzolino, V.; Algieri, C.; Calabrò, V.; Amar, R. Ben; Chakraborty, S. Graphene Oxide-Polysulfone Nanocomposite Membranes for Diclofenac Removal. *Emergent Mater.* **2024**, 1–15.
20. Chai, P. V.; Law, J.Y.; Mahmoudi, E.; Mohammad, A.W. Development of Iron Oxide Decorated Graphene Oxide (Fe3O4/GO) PSf Mixed-Matrix Membrane for Enhanced Antifouling Behavior. *J. Water Process Eng.* **2020**, *38*, 101673, doi:10.1016/j.jwpe.2020.101673.
21. Salah, Z.; Aloulou, H.; Aloulou, W.; Algieri, C. Development of Graphene Oxide Membrane on Flat Mud Ceramic Support for Methylene Blue Dyes Removal. **2025**, *202406142*, 1–11, doi:10.1002/slct.202406142.
22. Jacob, L.; Joseph, S.; Varghese, L.A. Polysulfone/MMT Mixed Matrix Membranes for Hexavalent Chromium Removal from Wastewater. *Arab. J. Sci. Eng.* **2020**, *45*, 7611–7620.
23. Bitinis, N.; Hernández, M.; Verdejo, R.; Kenny, J.M.; Lopez-Manchado, M.A. Recent Advances in Clay/Polymer Nanocomposites. *Adv. Mater.* **2011**, *23*, 5229–5236.
24. Ennaceri, H.; Mkpuma, V.O.; Moheimani, N.R. Nano-Clay Modified Membranes: A Promising Green Strategy for Microalgal Antifouling Filtration. *Sci. Total Environ.* **2023**, *902*, 166479.
25. Ko, I.; Ha, S.; Shin, W.H.; Choi, J.; Mun, S.C.; Choi, Y.; Won, J.H. Clay-Mineral-Coated Separators for Lithium-Ion Batteries: Exploring the Relationships between Clay Mineral Morphology and Separator Performance. *Adv. Sci.* **2025**, e10779.
26. Hikosaka, M.Y.; Pulcinelli, S.H.; Santilli, C.V.; Dahmouche, K.; Craievich, A.F. Montmorillonite (MMT) Effect on the Structure of Poly (Oxyethylene)(PEO)–MMT Nanocomposites and Silica–PEO–MMT Hybrid Materials. *J. Non. Cryst. Solids* **2006**, *352*, 3705–3710.
27. Ahmad, M. Bin; Gharayebi, Y.; Salit, M.S.; Hussein, M.Z.; Shameli, K. Comparison of in Situ Polymerization and Solution-Dispersion Techniques in the Preparation of Polyimide/Montmorillonite (MMT) Nanocomposites. *Int. J. Mol. Sci.* **2011**, *12*, 6040–6050.
28. Olad, A.; Rashidzadeh, A. Preparation and Anticorrosive Properties of PANI/Na-MMT and PANI/O-MMT Nanocomposites. *Prog. Org. Coatings* **2008**, *62*, 293–298.
29. Anadão, P.; Sato, L.F.; Wiebeck, H.; Valenzuela-Díaz, F.R. Montmorillonite as a Component of Polysulfone Nanocomposite Membranes. *Appl. Clay Sci.* **2010**, *48*, 127–132, doi:10.1016/j.clay.2009.12.011.
30. Hasani-Sadrabadi, M.M.; Dashtimoghadam, E.; Majedi, F.S.; Kabiri, K.; Solati-Hashjin, M.; Moaddel, H. Novel Nanocomposite Proton Exchange Membranes Based on Nafion® and AMPS-Modified Montmorillonite for Fuel Cell Applications. *J. Memb. Sci.* **2010**, *365*, 286–293.
31. Chailuecha, C. Methanol Barrier Layers: Modified Membrane Electrode Assemblies for the Improvement of Direct Methanol Fuel Cell Performance; The University of Manchester (United Kingdom), 2016; ISBN 1083569759.
32. Ali, F.; Ullah, H.; Ali, Z.; Rahim, F.; Khan, F.; Zia, U.R. Polymer-Clay Nanocomposites, Preparations and Current Applications: A Review. *Curr. Nanomater.* **2016**, *1*, 83–95.
33. Aseri, N.S.; Lau, W.J.; Goh, P.S.; Hasbullah, H.; Othman, N.H.; Ismail, A.F. Preparation and Characterization of Polylactic Acid-Modified Polyvinylidene Fluoride Hollow Fiber Membranes with Enhanced Water Flux and Antifouling Resistance. *J. Water Process Eng.* **2019**, *32*, 100912.
34. Anadão, P.; Sato, L.F.; Wiebeck, H.; Valenzuela-Díaz, F.R. Montmorillonite as a Component of Polysulfone Nanocomposite Membranes. *Appl. Clay Sci.* **2010**, *48*, 127–132.
35. Zinadini, S.; Zinatizadeh, A.A.; Rahimi, M.; Vatanpour, V.; Zangeneh, H. Preparation of a Novel Antifouling Mixed Matrix PES Membrane by Embedding Graphene Oxide Nanoplates. *J. Memb. Sci.* **2014**, *453*, 292–301, doi:10.1016/j.memsci.2013.10.070.
36. Yuliwati, E.; Ismail, A.F.; Matsuura, T.; Kassim, M.A.; Abdullah, M.S. Characterization of Surface-Modified Porous PVDF Hollow Fibers for Refinery Wastewater Treatment Using Microscopic Observation. *Desalination* **2011**, *283*, 206–213.
37. Fane, A.G.; Fell, C.J.D.; Waters, A.G. The Relationship between Membrane Surface Pore Characteristics and Flux for Ultrafiltration Membranes. *J. Memb. Sci.* **1981**, *9*, 245–262.
38. Zinadini, S.; Zinatizadeh, A.A.; Rahimi, M.; Vatanpour, V.; Zangeneh, H. Preparation of a Novel Antifouling Mixed Matrix PES Membrane by Embedding Graphene Oxide Nanoplates. *J. Memb. Sci.* **2014**, *453*, 292–301.

 doi:10.20944/preprints202510.1117.v1

39. Moradi, G.; Rahimi, M.; Zinadini, S. Antifouling Nanofiltration Membrane via Tetrathioterephthalate Coating on Aniline Oligomers-Grafted Polyethersulfone for Efficient Dye and Heavy Metal Ion Removal. *J. Environ. Chem. Eng.* **2021**, *9*, 104717.
40. Wang, Q.; Wang, X.; Fang, P.; Wang, D.; Dai, Y.; Wang, S.; Liew, K.M.; Xu, Z. Crystallization Behavior of Polypropylene/Polyamide 6/Montmorillonite Nanocomposites. *Polym. Int.* **2010**, *59*, 1303–1309.
41. Eversull, L.G.; Ferrell, R.E. Disordered Silica with Tridymite-like Structure in the Twiggs Clay. *Am. Mineral.* **2008**, *93*, 565–572.
42. Guo, X.; Yuan, H.; Xiao, T.; Wu, Y. Application of Micro-FTIR Spectroscopy to Study Molecular Association of Adsorbed Water with Lignin. *Int. J. Biol. Macromol.* **2019**, *131*, 1038–1043.
43. Caccamo, M.T.; Mavilia, G.; Mavilia, L.; Lombardo, D.; Magazù, S. Self-Assembly Processes in Hydrated Montmorillonite by FTIR Investigations. *Materials (Basel).* **2020**, *13*, doi:10.3390/ma13051100.
44. Madejová, J. FTIR Techniques in Clay Mineral Studies. *Vib. Spectrosc.* **2003**, *31*, 1–10.
45. Madejova, J.; Komadel, P. Baseline Studies of the Clay Minerals Society Source Clays: Infrared Methods. *Clays Clay Miner.* **2001**, *49*, 410–432.
46. Madejová, J.; Barlog, M.; Jankovič, L.; Slaný, M.; Pálková, H. Comparative Study of Alkylammonium- and Alkylphosphonium-Based Analogues of Organo-Montmorillonites. *Appl. Clay Sci.* **2021**, *200*, 105894.
47. Bărdacă Urducea, C.; Nechifor, A.C.; Dimulescu, I.A.; Oprea, O.; Nechifor, G.; Totu, E.E.; Isildak, I.; Albu, P.C.; Bungău, S.G. Control of Nanostructured Polysulfone Membrane Preparation by Phase Inversion Method. *Nanomaterials* **2020**, *10*, 2349.
48. Bergaya, F.; Lagaly, G. *Handbook of Clay Science*; Newnes, 2013; Vol. 5; ISBN 0080993710.
49. Kheirieh, S.; Asghari, M.; Afsari, M. Application and Modification of Polysulfone Membranes. *Rev. Chem. Eng.* **2018**, *34*, 657–693.
50. Anadão, P. Nanocomposite Filtration Membranes for Drinking Water Purification. In *Water purification*; Elsevier, 2017; pp. 517–549.
51. Alias, A.H.; Norizan, M.N.; Sabaruddin, F.A.; Asyraf, M.R.M.; Norrrahim, M.N.F.; Ilyas, A.R.; Kuzmin, A.M.; Rayung, M.; Shazleen, S.S.; Nazrin, A. Hybridization of MMT/Lignocellulosic Fiber Reinforced Polymer Nanocomposites for Structural Applications: A Review. *Coatings* **2021**, *11*, 1355.
52. Sand Chee, S.; Jawaid, M. The Effect of Bi-Functionalized MMT on Morphology, Thermal Stability, Dynamic Mechanical, and Tensile Properties of Epoxy/Organoclay Nanocomposites. *Polymers (Basel).* **2019**, *11*, 2012.
53. Wang, P.; Ma, J.; Wang, Z.; Shi, F.; Liu, Q. Enhanced Separation Performance of PVDF/PVP-g-MMT Nanocomposite Ultrafiltration Membrane Based on the NVP-Grafted Polymerization Modification of Montmorillonite (MMT). *Langmuir* **2012**, *28*, 4776–4786.
54. Wesén, E.V. Cellular Uptake of Amyloid Forming Proteins Related to Neurodegenerative Disease 2020.
55. Loske, L.; Nakagawa, K.; Yoshioka, T.; Matsuyama, H. 2D Nanocomposite Membranes: Water Purification and Fouling Mitigation. *Membranes (Basel).* **2020**, *10*, 295.
56. Chai, P. V; Law, J.Y.; Mahmoudi, E.; Mohammad, A.W. Development of Iron Oxide Decorated Graphene Oxide (Fe3O4/GO) PSf Mixed-Matrix Membrane for Enhanced Antifouling Behavior. *J. Water Process Eng.* **2020**, *38*, 101673, doi:https://doi.org/10.1016/j.jwpe.2020.101673.
57. Kumar, R.; Ismail, A.F. Fouling Control on Microfiltration/Ultrafiltration Membranes: Effects of Morphology, Hydrophilicity, and Charge. *J. Appl. Polym. Sci.* **2015**, *132*.
58. Wang, Q.; Wang, T.; Lv, Z.; Cui, M.; Zhao, Z.; Cao, X.; Wei, Q. TiO2 Sol-Gel Coated Pan/O-MMT Multi-Functional Composite Nanofibrous Membrane Used as the Support for Laccase Immobilization: Synergistic Effect between the Membrane Support and Enzyme for Dye Degradation. *Polymers (Basel).* **2020**, *12*, 139.
59. Nadour, M.; Boukraa, F.; Benaboura, A. Removal of Diclofenac, Paracetamol and Metronidazole Using a Carbon-Polymeric Membrane. *J. Environ. Chem. Eng.* **2019**, *7*, 103080.
60. Medhat Bojnourd, F.; Pakizeh, M. Preparation and Characterization of a PVA/PSf Thin Film Composite Membrane after Incorporation of PSSMA into a Selective Layer and Its Application for Pharmaceutical Removal. *Sep. Purif. Technol.* **2018**, *192*, 5–14, doi:https://doi.org/10.1016/j.seppur.2017.09.054.

 doi:10.20944/preprints202510.1117.v1